Nucleotide excision repair at the single-molecule level : analysis of the E. coli UvrA protein

Wagner, K.

Recognition of DNA damage in Real-Time: Observing the interaction of UvrA with DNA using single-molecule Fluorescence Microscopy

Chapter 3

Koen Wagner[1], Peter Gross[2], Andreas Biebricher[2], Erwin J. Peterman[2], Gijs J. Wuite[2], John van Noort[3], Geri F. Moolenaar[1] and Nora Goosen[1]

[1]Laboratory of Molecular Genetics, Leiden Institute of Chemistry, Leiden University, Einsteinweg 55, 2333 CC, Leiden, the Netherlands
[2]Department of Physics and Astronomy and Laser Centre, Vrije Universiteit, 1081 HV Amsterdam, The Netherlands
[3]Physics of Life Processes, Leiden Institute of Physics, Leiden University, Niels Bohrweg 2, 2333 CA, Leiden, the Netherlands

ABSTRACT

UvrA is the initial DNA damage-sensing protein in bacterial nucleotide excision repair and detects a wide variety of lesions. To facilitate removal of lesions from the bacterial genome, UvrA needs to accurately discriminate between DNA damage lesions from undamaged DNA. In this study, we investigated the damage discrimination mechanism of UvrA by observing the interaction of single UvrA complexes with DNA in real-time using two different single-molecule fluorescence microscopy imaging techniques: Total Internal Reflection Fluorescence (TIRF) and farfield fluorescence microscopy. With TIRF-microscopy we have observed UvrA binding to surface-tethered DNA. With farfield fluorescence microscopy we have observed UvrA binding to DNA tethered between two optically trapped beads. Farfield fluorescence microscopy had the advantage of observing DNA sufficiently for away from a surface which can cause complications.

Imaging with TIRF-microscopy, which requires proteins to interact with DNA anchored close to a flow cell surface, was greatly hampered by non-specific surface adsorption. Initial results however suggest that in the presence of ATP UvrA had bound to preferential sites along the DNA substrate. Although in the presence of ATP no searching UvrA complexes were detected, the results indicate that in this condition the search for DNA damage should be a very fast process. Under optimal conditions, UvrA could find the present preferential sites in a 48 kb long DNA substrate within 20 seconds. When ATPγS, a non-hydrolyzable ATP analog, is used UvrA is less specific for DNA damage; our results suggest that in this condition UvrA binds longer to non-specific sites.

INTRODUCTION

The UvrA protein is the initial sensor for DNA damage in bacterial NER. The unique feature of UvrA is that it detects a wide variety of structurally and chemically unrelated DNA lesions (reviewed in [1]). In order to find these few lesions in the bacterial genome, which essentially is a long chain of undamaged DNA, UvrA has to efficiently discriminate between undamaged and damaged DNA. Therefore, the detection of DNA damage has to be both an accurate (undamaged DNA should not be recognized as damage) and a fast process (DNA damage should be repaired before it can interfere with cellular processes). Understanding the mechanism by which proteins search for specific DNA binding sites is a fundamental question in biochemistry. Essentially all biological functions of DNA are the result of proteins interacting with target sites, such as specific sequences or base modifications [2].

Pioneering work on a sequence specific DNA binding protein, the *E. coli lac* repressor, proposed that site-specific DNA binding proteins do not find their target sequence by binding and dissociating from random sites alone (3D-diffusion), but instead also by a process termed ‘facilitated diffusion’ [3-5]. The facilitated diffusion model proposes, apart from binding and dissociation on random DNA sites, two extra modes of interaction, which greatly enhance the efficiency of recognition of a specific binding site: 1D-diffusion along DNA (sliding) and relocation through simultaneously binding two non-specific sites (intersegmental transfers). Sliding along non-specific sites greatly increases the search efficiency as this would allow a protein to test multiple non-specific sites during one binding event. An intersegmental transfer increases the search efficiency by allowing fast translocation of a protein between DNA sites that are distant by sequence, but are not spatially distant [2,6].

With the emergence of single-molecule techniques, the different modes of DNA interaction can now be directly detected. Thus, 1D-diffusion along DNA has been demonstrated for sequence specific DNA binding proteins [7,8] and for the DNA repair protein hOgg1, which recognizes oxidative lesions in the DNA [9], and the protein complex Msh2-Msh6, which recognizes DNA mismatches [10]. In this study, we have explored the search mechanism of UvrA. For this purpose we have used two different, but complementary strategies to directly UvrA binding to DNA: nearfield Total Internal Reflection Fluorescence (TIRF) microscopy and farfield epi-fluorescence microscopy.

TIRF-microscopy utilizes the features of an induced evanescent wavefield to selectively illuminate fluorophores in a restricted area, thereby reducing the background signal from fluorophores outside the evanescent field. An evanescent wavefield is created when the incident laser beam is totally reflected at a glass-water interface (the surface of a flow cell). The evanescent wavefield decays exponentially in the water layer and penetrates the water layer to a depth of approximately 100 nm [11]. Therefore, only fluorophores that are present close to the flow cell surface can be excited. To allow visualization of UvrA binding to DNA in real-time with TIRF-microscopy, DNA needs to be tethered to the glass surface of a flow cell. This was achieved through coupling both biotinylated ends of a DNA molecule to a modified glass surface, which is sparsely coated with neutravidin, finally creating a DNA substrate that is coupled to the surface at both ends (Figure 1).

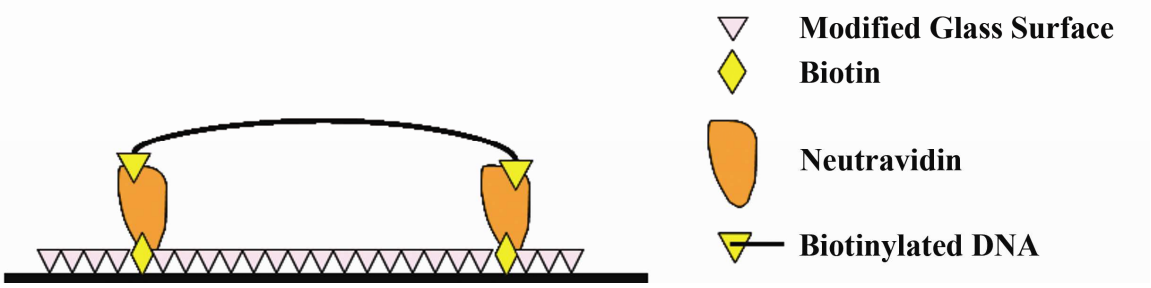

Figure 1: The DNA substrate used for TIRF-microscopy
Both ends of the DNA substrate are targeted to a modified glass surface, using biotin-neutravidin coupling and flow stretching of DNA. The DNA is tethered to the surface at both ends. In this conformation, the tethered DNA is still mobile not fully stretched along the surface.

With farfield epi-fluorescent microscopy we have imaged UvrA binding to DNA, which was immobilized inside a flow cell. This was done by coupling both biotinylated ends of a DNA molecule to streptavidin coated beads. These beads can be optically trapped, generating a DNA molecule that is immobilized in solution. By pulling on one trapped bead, the tension on the DNA can be varied (Figure 2).

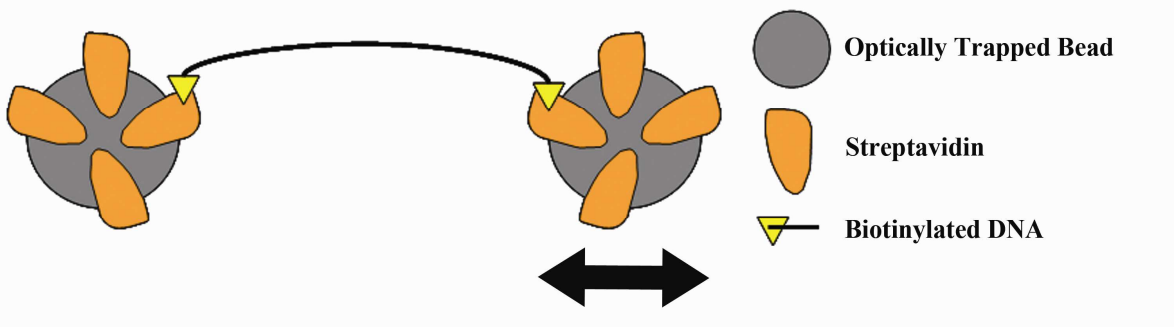

Figure 2: The DNA substrate used for surface-free imaging of UvrA binding DNA
DNA is tethered between two optically trapped beads using biotin-streptavidin coupling.

Although both techniques were demonstrated to be very well suited for imaging protein-DNA interactions at single-molecule level in real time [8-10,12], each of these two strategies has its very specific advantages and disadvantages (reviewed in [13]). In short, the advantage of TIRF-microscopy is that multiple DNA molecules can be imaged simultaneously and that relatively low concentrations of protein (pM concentration) can be used.
The major disadvantage of using TIRF is, however, that it requires surface modification, which makes sample preparation more elaborate and time-consuming. Furthermore, adsorption of DNA, protein or fluorescent contaminants to the surface can be a problem. The advantage of imaging a protein binding to DNA coupled to two optically trapped beads is that the DNA can be immobilized in solution and therefore does not require time-consuming surface modifications. Furthermore, protein and DNA can be imaged sufficiently far away from the flow-cell surface, which eliminates non-specific interactions with the flow-cell surface. The disadvantages of the optical trap system, however, are that only one DNA molecule can be imaged per incubation and that a higher protein concentration (nM concentration) needs to be used. Also, in our experiments farfield fluorescence imaging was done at a slower rate (500 ms/image) than what could be achieved with TIRF-microscopy (100 ms/image or faster).

In this chapter, we describe sample preparation and imaging conditions for both techniques in more detail as well as present initial results obtained with UvrA. In our experiments, we were able to detect single UvrA-complexes binding DNA, both with TIRF- and farfield-microscopy. These UvrA complexes were functional, as their activity clearly changed when a different cofactor (ATP or ATPγS) was used.

Unexpectedly, we found that in the presence of ATP most of the observed UvrA complexes did not display any sliding motion along the DNA, but instead remain stably bound to their binding site. Likely, these UvrA complexes are bound to preferential binding sites that are present in the DNA substrate.

In the presence of ATPγS, we have observed UvrA binding to non-specific sites. In this experiment the majority of UvrA complexes bound stably and did not slide along DNA. A few events were observed, in which UvrA moved between different DNA sites. The number of these events however was too small to deduce their relevance to the repair mechanism.

MATERIALS AND METHODS

Labeling and purification of fluorescent UvrA and UvrB

UvrA and UvrB were purified in a buffer suitable for amino-specific labeling (0.2 M KPO_4, pH 8.0 in 20 % glycerol). Cy5-NHS (GE Life Sciences) powder was dissolved in anhydrous DMSO, in a final concentration of 10 mM. Amino-specific labeling of UvrA was performed by addition of 100 μM Cy5-NHS to 2 μM UvrA in labeling buffer, followed by overnight incubation in the dark, at 4 °C. UvrB was labeled with Cy5-NHS in the same conditions, using 400 μM Cy5-NHS and 20 μM UvrB.

The attachment of Cy5 to UvrA was verified by SDS-PAGE (an amount of ~10 pmol of Cy5 on a gel is visible with the naked eye). Unreacted dye was removed from the solution using a Blue-Agarose column. After elution of the Cy5-labeled UvrA from the Blue-Agarose column, Cy5-UvrA was dialyzed overnight (4 °C, in the dark) against UvrA-storage buffer (50 mM Tris-HCl, pH 7.5, 300 mM KCl, 1 mM EDTA, 10 mM β-mercaptoethanol and 2 mM benzamidine in 20 % glycerol). Subsequently, the concentration of the protein was determined with SDS-PAGE.

A similar protocol was used to couple Cy5-NHS to UvrB, except that here unreacted dye was separated from the fluorescent UvrB using a PD-10 desalting column (Amersham).

The average degree of labeling of purified Cy5-labeled protein was determined spectrophotometrically.

Mass Spectrometry

Prior to mass spectrometry analysis, Cy5-UvrA was precipitated in 20 % trichloroacetic acid (1 h, 4 °C). The precipitated protein was resuspended in 8 M urea + 0.4 M NH_4HCO_3 and subsequently treated with 45 mM DTT (15 min, 50 °C) and 100 mM iodoacetamide (15 min, room temperature). After treatment, Cy5-UvrA was digested with trypsin (24 h, 37 °C). After trypsin digestion, the fragmented protein was desalted and purified with a $ZipTip_{C18}$ desalting pipette tip (Millipore).

Mass spectrometry was performed on a Finnigan LTQ OrbiTrap nanospray LC/MS mass spectrometer (Thermo Scientific). Mass spectrometry data were analyzed with the analysis program SEQUEST (Thermo Finnigan).

DNA substrates and Biochemical assays

DNA oligomers were purchased from EuroGentec.

The 50 and 96 bp substrates, containing a Fluorescein-dR (6-Fluorescein, Glen Research) lesion, were constructed and radioactively labeled as described [14].

The 678 bp DNA fragment with a CPD lesion incorporated at position 340 was prepared as described [15].

For the TIRF-microscopy experiments, biotinylated λ-phage DNA was made by filling up both ss-DNA ends of λ-phage DNA (Roche) with Klenow polymerase as described [16], replacing dTTP with Biotin-11-dUTP (Fermentas). In the optical trap-based experiments, commercially available biotinylated λ-phage DNA (Invitrogen) was used.

Gel retardation assays [17] and Atomic Force Microscopy [18] were performed as described.

Surface modification techniques

Prior to coating, cover slides were cleaned as described [19,20]. In short, glass cover slides (Assistant, Germany) were sonicated in 1 % RBS-50 anionic detergent for 15 minutes, rinsed with MilliQ water, sonicated for 1 hour in ethanol (96 %), rinsed with MilliQ water, flame-dried and placed for 1 hour in a UVO UV ozone cleaning device (Jelight, USA). After this cleaning procedure, no background fluorescence could be detected on the glass slides. To couple DNA to the flow cell surface, but also to reduce surface adsorption of DNA and proteins, three different surface modifications techniques were tried.

1. Linear PEG

Prior to PEG coating, cleaned glass slides were amino-functionalized with either poly-D-lysine (as described [19 and 20]) or aminopropyl-triethoxysilane (APTES) (as described in [8]). Amino-functionalized slides were subsequently incubated (at least 4 h, room temperature) with a mixture of amine reactive PEG derivatives, consisting of 20 % mPEG-succinimidyl prioponate 5.000 MW (Nektar Therapeutics) + 0.2 % biotin-PEG-*n*-hydroxy-succinimide 3.400 MW (Nektar Therapeutics) in 0.1 M sodium carbonate (pH 8.2), as described [19,20]. PEG coated coverslides were stored under vacuum, in the dark, for up to a month.

2. Star-PEG

Star-PEG coating of cover slides was done exactly as described [20]. In short, six arm NCO PEG stars (MW 12 kDa) (described in [21]) were dissolved in tetrahydrofuran at a concentration of 20 mg/ml and diluted in MilliQ-water to a concentration of 2 mg/ml. Biocytin (Sigma) was added to a final concentration of 1 μg/ml. Five minutes after the mixing, the solution was filtered through a 0.22 μm syringe filter (MilliQ) and deposited onto an amino-functionalized clean coverslide.

When the slide was fully covered with star-PEG solution, the slide was spin coated for 45 seconds at 2500 rpm. Before use, the slides were incubated overnight at room temperature (RT) in the dark to complete the cross-linking reaction of star-PEG. Star-PEG coated coverslides were stored at RT in the dark for up to one week.

3. BSA + Neutravidin coating

Coating of the glass slide surface with BSA and neutravidin was accomplished inside the flow cell (see below) by incubating (3 h, RT) the flow cell with a solution of 50 mM Tris-HCl (pH 7.5), 100 mM KCl and 10 mM $MgCl_2$ containing 2 % BSA (w/v) and 50 – 100 μg/ml neutravidin. To reduce surface adsorption of proteins, further surface blocking was done with 2 % acetylated BSA + 2 % casein (2 h, RT). After incubation with this buffer, the coated flow cell was washed with 300 μl 1x endo buffer (50 mM Tris-HCl, pH 7.5, 50 mM KCl, 10 mM $MgCl_2$ + 0.01 % (w/v) BSA).

Surface tethering of DNA

A flow cell was assembled by sealing a poly-dimethylsiloxane (PDMS) channel with a functionalized glass slide. The size of the used flow cells was 50 x 2 x 0.15 mm. The flow cell temperature was stabilized at 37 °C using a water circulating bath.

Before the addition of neutravidin, the flow cell was washed with 500 μl 1x endo buffer. Prior to use, this buffer was filtered through a 0.02 μm syringe filter (Whatman) and degassed. Proteins and DNA were later added to the filtered and degassed buffer.

On the linear PEG and starPEG coated surfaces, neutravidin (Roche) was attached to biotin by adding 300 μl neutravidin solution (10 ng/ml neutravidin in 1x endo buffer) to the flow cell. The neutravidin solution was incubated for 10 min. Subsequently, the flow cell was washed with 300 μl 1x endo, before 500 μl biotinylated λ-phage DNA (50 ng/ml in 1x endo buffer) was flushed in. The DNA solution was incubated on the neutravidin coated surface for 10 min. On the BSA + neutravidin coated surface, biotinylated λ-phage DNA was added to the flow cell directly after the coating and blocking steps.

After incubating DNA on the neutravidin surface, DNA is attached to the surface on one end. Coupling of the second biotinylated DNA end to the surface was done by stretching the DNA along the surface using a buffer flow. For this purpose, the flow cell was washed for 10 min with 1x endo, using a continuous flow speed of 3 µl/sec.

Binding of UvrA to surface-tethered DNA

300 µl 1x endo containing 25 pM Cy5-UvrA was added to the flow cell, with a continuous flow of 3 µl/sec. When indicated, ATP (Roche) was present in a concentration of 1 mM.
To protect Cy5-UvrA from bleaching, an oxygen scavenging system, consisting of glucose oxidase (4 µg/ml) (Sigma), catalase (0.8 µg/ml) (Fluka) and β-D glucose (0.08 w/v %) (Sigma), was included and 0.4 mM Trolox (Sigma) was added as a blinking suppressant.
Images of UvrA were recorded as soon as fluorescent spots were visible. Imaging was continued for 10 min after buffer flow had stopped.
After recording images of Cy5-UvrA, the flow cell was washed with 300 µl low-Mg^{2+} buffer (50 mM Tris-HCl, pH 7.5, 50 mM KCl + 2 mM $MgCl_2$). The same buffer plus 1 nM YOYO-1 (Invitrogen) was subsequently added to stain the DNA. A buffer with a low magnesium concentration was used, because a too high concentration of Mg^{2+} interferes with the intercalation of YOYO-1 [22].

TIRF Microscopy

TIRF-microscopy single-molecule fluorescence experiments were performed on a setup described in [19]. In short, molecules were imaged on a CCD camera (Cascade 512B, Roper Scientific) through a home-built inverted total internal reflection microscope with an oil immersion objective (100X, 1.45 NA, NIKON). The flow cell surface was alternately excited with 514 nm and 636 nm laser lines through an AOTF (A.A. Opto-Electronic). Fluorescence (from either of both laser lines) was imaged simultaneously on separate areas of the CCD chip using a dichroic mirror wedge, as previously described (Cognet et al., 2000). Unless indicated otherwise, images were recorded with an acquisition rate of 1 image per 100 ms. The freeware program ImageJ [24] was used for image analysis and to generate screenshots and kymographs.

Imaging of UvrA with wide-field fluorescence microscopy

A four channel flow cell (Figure 3) was constructed by melting three parafilm slides together. In our experiments, this flow cell was not temperature controlled; therefore our experiments were performed at room temperature (20 °C).

Experiments were performed on a set-up combining double optical tweezers with epi-fluorescence detection described in [12].

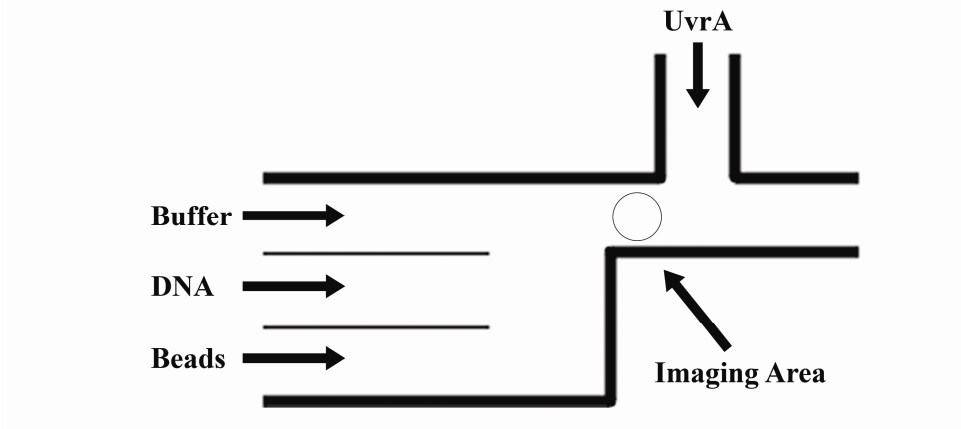

Figure 3: The flow cell used in the optical trap experiments. Imaging is done at the junction between the buffer and the UvrA channel (indicated with the red arrow). At this position there is laminar buffer flow.

Streptavidin coated beads are flushed into the flow channel and, eventually, two of them will be trapped by the two optical traps. The trapped beads are transported to a new flow channel where biotinylated λ-phage DNA is flushed in, resulting in the coupling of DNA to a trapped bead. Tethering of the biotinylated DNA to the second trapped bead is accomplished by applying buffer flow. The presence and integrity of the DNA tethered between both beads is verified by recording the stretching force required to pull both beads apart.

To allow UvrA binding, the beads are transported to the UvrA channel, which contains 2.5 nM UvrA in 1x endo. When indicated, ATP or ATPγS (Roche) was present in a concentration of 1 mM. The tethered DNA was incubated for the indicated amount of time, ranging between 1 and 200 sec. Incubation was done during continuous buffer flow.

Before imaging of the DNA bound UvrA, the beads are transported back to the buffer channel, containing 1x endo plus oxygen scavengers. This is done to minimize the background signal of non-DNA bound fluorescent proteins. This step however does introduce a short delay time (approximately 5 sec) between incubation and imaging. Imaging was done during continuous buffer flow. Unless indicated otherwise, images were recorded with an acquisition rate of 1 image per 500 ms. The freeware program ImageJ [24] was used for image analysis and to generate screenshots and kymographs.

RESULTS

Preparation of fluorescent UvrA and UvrB

The labeling of UvrA with Cy5 resulted in a 0.5 μM sample, with an average degree of labeling of 1.2 Cy5 per monomer UvrA. An average degree of labeling of 1.2 indicates that the majority of Cy5-UvrA used in this study likely contains 0, 1 or 2 Cy5-molecules per monomer UvrA. With mass spectrometry, we tried to identify the residue Cy5 was coupled to. Although conditions were chosen to favor labeling of the N-terminus of UvrA, we did not find any Cy5 attached to the N-terminus of UvrA. However, we did find evidence for Cy5-labeling on amino acids K191 and K210, although their occurrence was too low to conclude that Cy5-UvrA has exclusively coupled to these sites. Therefore, we assume that the Cy5 in our Cy5-UvrA is randomly attached to exposed lysine residues, of which Cy5-K191 and Cy5-K210 form a large sub-population. K191 and K210 are both surface exposed amino acids that are part of the UvrB binding domain of UvrA. Neither residue is conserved between UvrA proteins from different species. Cy5-UvrB was purified with a concentration of 10 μM and an average degree of labeling of 2.8 Cy5 per UvrB monomer. The position of the label(s) on UvrB was not determined.

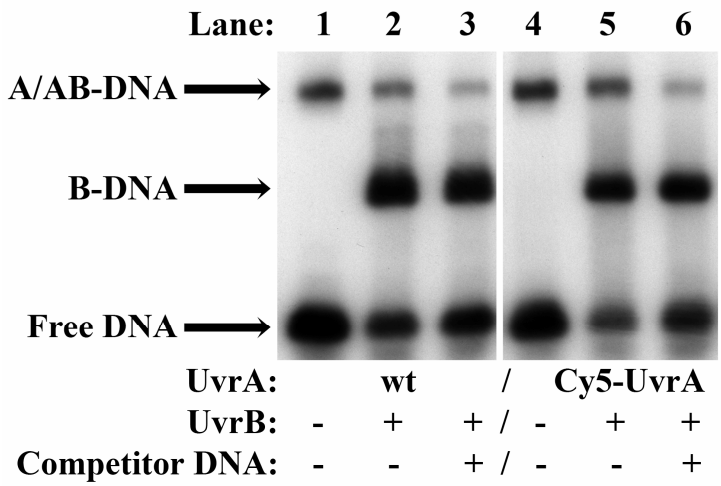

Figure 4: DNA binding and UvrB-loading activity of Cy5-UvrA

1.25 nM UvrA was incubated with 0.36 nM DNA (50 bp, containing a Menthol lesion). When indicated, UvrB was used in a concentration of 100 nM.

200 ng pUC18 plasmid DNA was added to the sample as competitor DNA. 200 ng DNA equals an 3000 times excess (in basepairs) of competitor DNA over the 50 bp DNA substrate.

All reactions were done in 1x endo buffer containing 1 mM ATP. The reaction mixtures were separated on a 3.5 % polyacrylamide native gel containing 10 mM $MgCl_2$ and 1 mM ATP. Arrows indicate the positions of UvrA-bound DNA, UvrB-bound DNA and free DNA.

Characterization of Cy5-labeled UvrA and UvrB

The DNA binding activity of Cy5-labeled UvrA and its ability to load UvrB on damaged DNA were tested in a gel shift assay (Figure 4). The results show that the DNA binding activity of Cy5-UvrA alone and its ability to load UvrB were not significantly different from non-labeled UvrA (Figure 4). The ability of Cy5-UvrA to discriminate DNA damage was further tested by determining the efficiency of loading UvrB to damaged DNA in the presence of a large excess of undamaged competitor DNA. In this assay, both Cy5-UvrA and non-labeled UvrA loaded a similar amount of UvrB to the damaged DNA (Figure 4, lanes 3 and 6). Taken together, the purified Cy5-UvrA has activity similar to non-labeled UvrA and is therefore of a sufficient quality for use in single-molecule fluorescence imaging assays. However, it should be noted that, although the bulk of the Cy5-UvrA functions like non-labeled UvrA, the purified Cy5-UvrA is a mixture of different UvrA molecules with Cy5-labels at variable positions. Therefore, it could be that a small population within the Cy5-UvrA exists that has a different activity.

The DNA-binding activity of the Cy5-labeled UvrB was also tested with a gel retardation assay. These results however revealed that Cy5-UvrB had a significantly reduced activity compared to non-labeled UvrB (data not shown). Likely, the coupling of a fluorescent dye to an exposed amine-group in UvrB affects activity and for this reason Cy5-UvrB was not used for fluorescence imaging experiments.

Activity of UvrA and UvrB in the presence of oxygen scavengers

Because single-molecules fluorescence imaging requires the use of an oxygen scavenging system to suppress bleaching and blinking of the fluorophore, the effect of the oxygen scavenging system on the DNA binding activity of UvrA and UvrB was tested in a gel shift assay (Figure 5). First, we tested the effect of the oxygen scavenging system in the concentration used by Koopmans *et al.* [20]. With this concentration, only a slight inhibition of DNA binding by UvrA was observed (Figures 5A and 5B, lanes 5 and 6), but the loading of UvrB was greatly reduced (Figure 5C, lanes 4-6). When a 5-fold lower concentration of oxygen scavengers was used, DNA binding of UvrA (Figures 5A and 5B, lanes 3 and 4) or the loading of UvrB (Figure 5C, lanes 1-3) was not significantly inhibited. With this lower concentration of oxygen scavengers, no bleaching of surface-adsorbed Cy5 was detected in the first 10 sec of TIRF imaging (data not shown).

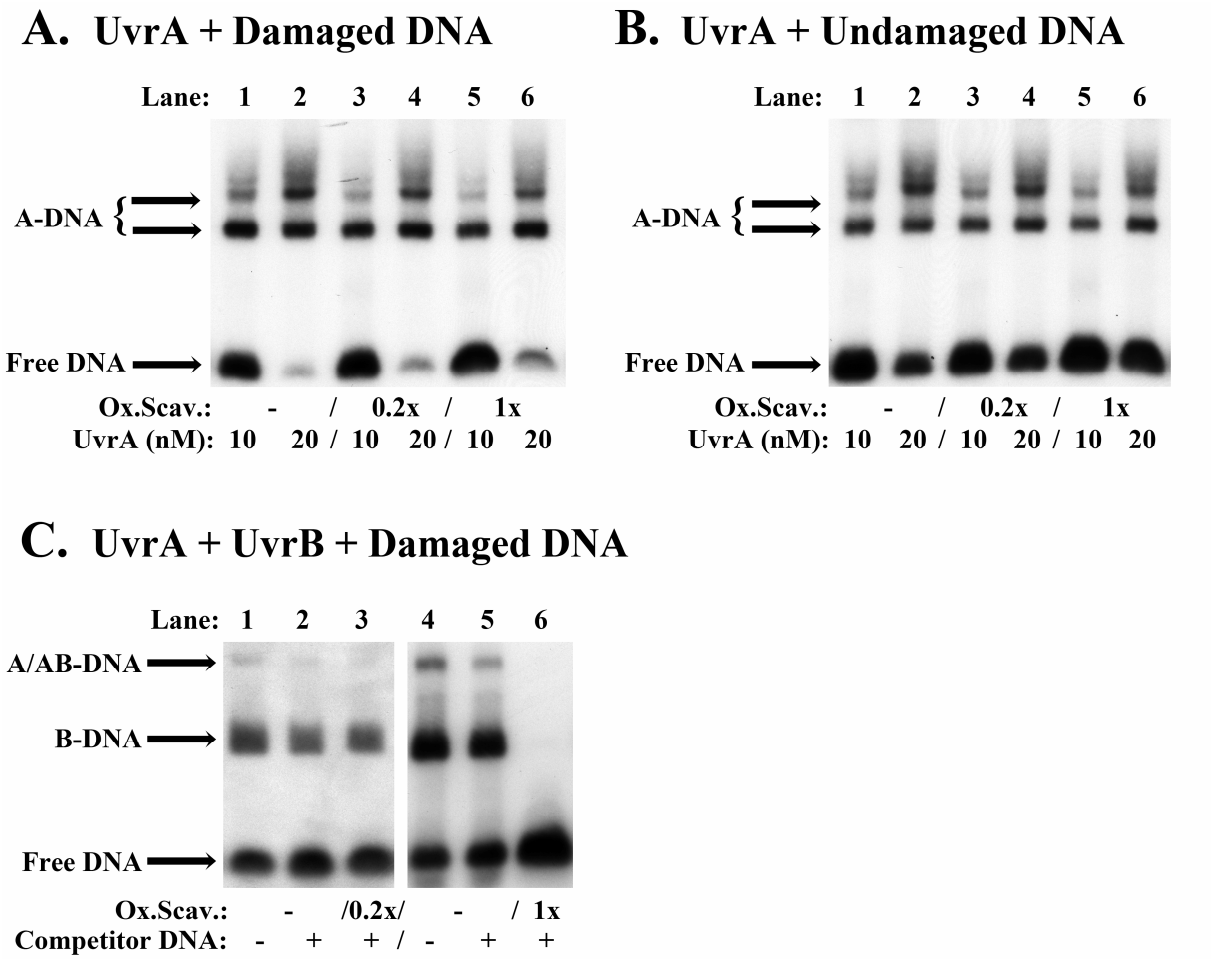

Figure 5: Effect of oxygen scavenging system on DNA binding activity of UvrA and UvrB

(**A**) UvrA binding to damaged DNA and (**B**) undamaged DNA

UvrA (10 – 20 nM) was incubated with 2 nM undamaged or damaged DNA (96 bp, Fluorescein-dR damage).

(**C**) Loading of UvrB to damaged DNA

1.25 nM UvrA and 100 nM UvrB were incubated with 0.36 nM DNA (50 bp, containing a Menthol lesion). When indicated, 200 ng plasmid DNA (pUC18) was added as competitor DNA.

A 1x concentrated oxygen scavenging system consists of 2 mM Trolox, 0.4% β-D-glucose, 20 μg/ml glucose oxidase and 4 μg/ml catalase. All reactions were done in 1x endo buffer containing 1 mM ATP. The reaction mixtures were separated on a 3.5 % polyacrylamide native gel containing 10 mM $MgCl_2$ and 1 mM ATP. Arrows indicate the positions of UvrA-bound DNA, UvrB-bound DNA and free DNA.

Activity of UvrA and UvrB at room temperature

Because tethering of DNA between optically trapped beads could only be performed at room temperature, we determined the activities of UvrA and UvrB in this condition. First, we tested the overall affinity of UvrA for DNA at room temperature with a gel shift assay, finding no obvious differences in DNA affinity between room temperature and 37 °C (Figure 6A and 6B). Next, we tested the effect of temperature on damage specific binding of UvrA in more detail, using AFM, by determining the specificity for CPD lesions and DNA ends.

At room temperature UvrA had the same specificity for CPD-DNA as at 37 °C (Table 1) and also its specificity UvrA for DNA ends was not affected (Table 2). The specificity of Cy5-UvrA for DNA ends at room-temperature was also determined. In the presence of ATP, Cy5-UvrA had a similar specificity for DNA ends as non-labeled UvrA (Table 2). In the presence of ATPγS however, Cy5-UvrA showed a lower specificity for DNA ends; about 10 % less Cy5-UvrA was found at a DNA end (Table 2). These results indicate that the presence of a fluorescent label on UvrA can interfere with DNA binding, but only when UvrA has bound ATPγS. Possibly, the label could be attached to amino acids that make contact with DNA when ATPγS is bound to UvrA.

Table 1: Site-specific binding of UvrA on CPD-DNA at 37 °C and RT

Cofactor	% on Damage	% On End	% On Non-specific Site
UvrA wildtype, 37 °C			
ATP	46.3 ± 4.8	28.4 ± 0.6	25.3 ± 5.3
UvrA wildtype, Room Temperature (20 °C)			
ATP	44.2 ± 4.0	20.3 ± 2.7	35.5 ± 2.1

UvrA was incubated with a 678 bp DNA fragment containing a CPD lesion in the center and the complexes were visualized by AFM. The percentage of complexes bound at a specific site was calculated as described [18].

Table 2: Site-specific binding of UvrA and Cy5-UvrA on undamaged DNA at 37 °C and RT

Cofactor	% On End	% On Non-specific Site
UvrA wildtype, 37 °C		
ATP	50.5 ± 4.5	49.5 ± 4.5
ATPγS	54.2 ± 6.9	45.8 ± 6.9
UvrA wildtype, Room Temperature (20 °C)		
ATP	55.6 ± 5.9	44.4 ± 5.9
ATPγS	49.5 ± 7.0	50.5 ± 7.0
Cy5-UvrA, Room Temperature (20 °C)		
ATP	59.3 ± 7.4	40.7 ± 7.4
ATPγS	39.6 ± 3.8	60.4 ± 3.8

UvrA was incubated with a 678 bp undamaged DNA fragment and the complexes were visualized by AFM. The percentage of complexes bound at a DNA end was calculated as described [18].

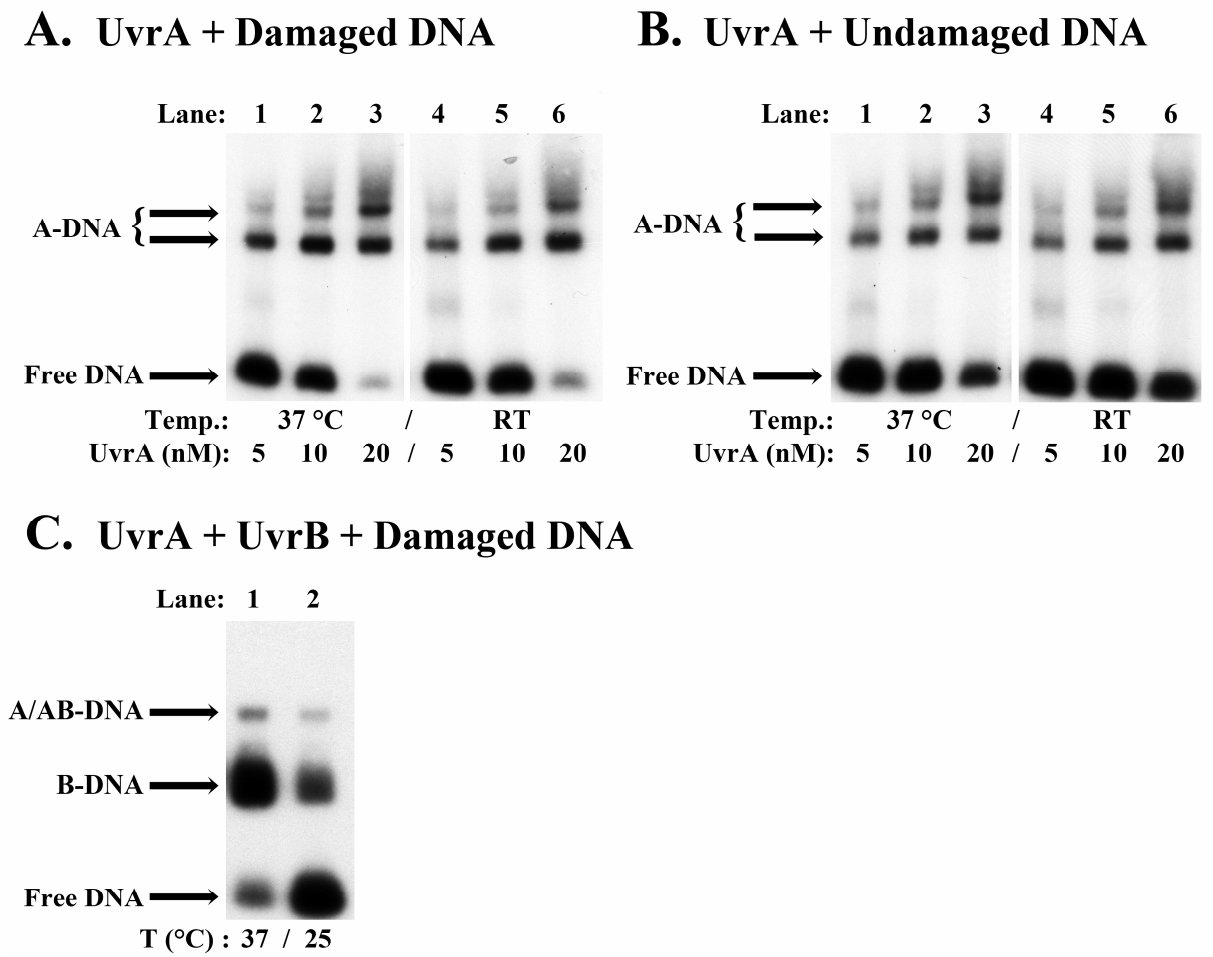

Figure 6: Activity of UvrA and UvrB at reduced temperature

(**A**) UvrA binding to damaged DNA and (**B**) undamaged DNA

UvrA (5 – 20 nM) was incubated with 2 nM undamaged or damaged DNA (96 bp, Fluorescein-dR damage). Room Temperature was 20 °C

(**C**) Binding of UvrA and UvrB to damaged DNA

UvrA (1.25 nM) and UvrB (100 nM) were incubated with 1 nM damaged DNA (50bp, Fluorescein-dR damage). All reactions were done in 1x endo buffer containing 1 mM ATP. The reaction mixtures were separated on a 3.5 % polyacrylamide native gel containing 10 mM $MgCl_2$ and 1 mM ATP. Arrows indicate the positions of UvrA-bound DNA, UvrB-bound DNA and free DNA.

In contrast to the damage specificity of UvrA, loading of UvrB onto damaged DNA was compromised at room temperature. At 25 °C, the loading of UvrB to damaged DNA was dramatically reduced compared to 37 °C (Figure 6C). This is likely correlated to the reduced ATPase activity of UvrB at room temperature (data not shown). Based on these results we conclude that fluorescence imaging experiments with UvrA alone can be done at room temperature, but the loading of UvrB to damaged DNA should best be imaged at 37 °C. We have however not tried this due to the reduced activity of the labeled UvrB.

Imaging UvrA binding DNA with TIRF microscopy

To observe DNA binding by UvrA with TIRF microscopy, we added UvrA (25 pM) and ATP to a flow cell containing surface tethered DNA. The addition of UvrA into the flow cell (lasting about 100 seconds) created a buffer flow along the DNA. Initial experiments with YOYO-stained DNA indicated that buffer flow affected the conformation of the surface-tethered DNA. In the absence of buffer flow, the surface-tethered DNA appeared to move in and out the evanescent field, while during buffer flow the DNA is stretched along the surface (after buffer flow stopped, the DNA reverted to its original 'jump rope' conformation (shown in Figure 1)). The presence of buffer flow however did not have a significant effect on the binding of UvrA. Imaging of fluorescent complexes was continued for 10 minutes after all UvrA had been added to the flow cell, then the flow-cell was stained with DNA dye YOYO-1. Figure 7A shows an example image of Cy5-UvrA, in this field of view about 15 Cy5-UvrA molecules are visible; the presence of DNA was verified by staining the DNA with YOYO-1 directly after imaging (Figure 7B). On the merged image (Figure 7C) it can be seen that three Cy5-UvrA spots overlap with the position of YOYO-DNA, demonstrating the interaction of UvrA with DNA.

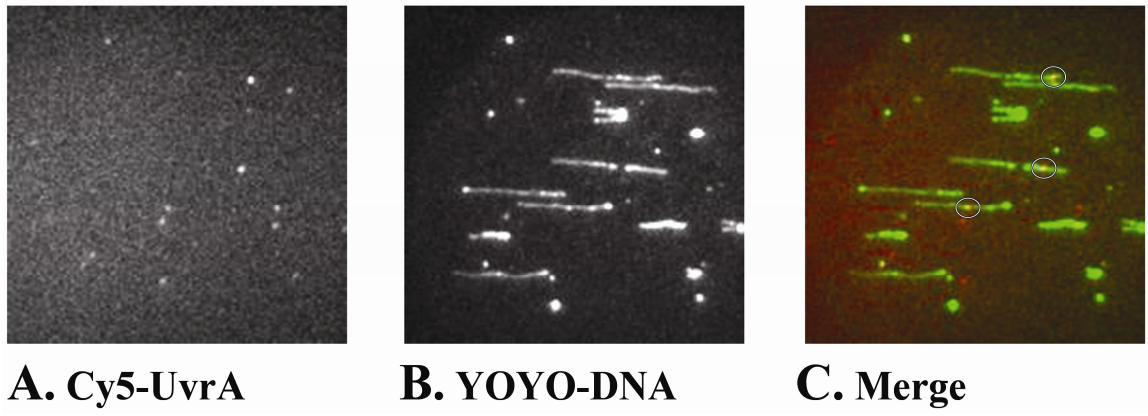

Figure 7: Detection of UvrA binding to surface-tethered DNA
Images of (**A**) Cy5-UvrA and (**B**) YOYO-1 stained surface-tethered DNA taken from the same field of view (size: 30 × 30 μm) and (**C**) merged image of both panels (DNA = green, UvrA = red).
Cy5-UvrA complexes that have bound to DNA (colored yellow) are indicated with white circles.

To detect any changes in the position of the DNA-bound UvrA-complexes, kymographs were made from all the images of Cy5-UvrA molecules, which appeared to have bound DNA. (a kymograph gives a graphical representation of position over time, in which one spatial axis represents time). Examples of these kymographs are shown in Figure 8. The most commonly observed behaviour of UvrA was a stationary and stable DNA binding. An example of such a complex is shown in Figure 8A.

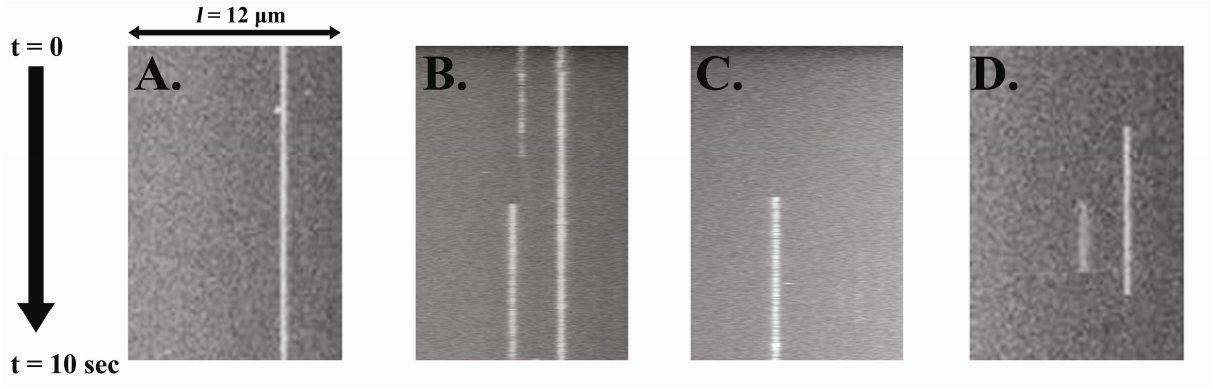

Figure 8: Example kymographs of UvrA bound to surface-tethered DNA

All shown kymographs were taken from images of Cy5-UvrA, incubated at 37 °C, in the presence of ATP and a 1x concentrated oxygen scavenging system. The surface-tethered DNA had a length of approximately 12 µm, which is the shorter than length of stretched λ-phage DNA (48,000 bp), indicating that the DNA was not fully stretched along the surface. The kymographs were made using ImageJ software.

These complexes had already bound to DNA before imaging had started and remained at the same position for the entire imaging sequence (here: 10 seconds). About 90 % of the approximately 80 observed DNA bound UvrA complexes behaved this way. Some of these complexes disappeared during imaging. An example of such a complex is shown in Figure 8B. The disappearance of the UvrA indicates that the complex dissociated from the DNA, as under these imaging conditions fluorophore bleaching did not occur within the first 10 seconds of imaging (data not shown).

The long lifetime and immobility of the UvrA complex is unexpected, as it would be impossible for UvrA to efficiently locate DNA lesions through binding each single DNA site for 10 seconds or longer. Therefore, these complexes might have bound to preferential binding sites within the DNA substrate. Although we could not define the exact nature of these sites, these preferential sites are likely DNA damage (such as DNA nicks, oxidative lesions or aberrant DNA structures) created during preparation of the biotinylated λ-DNA (here, we will refer to these unknown damages as ‘preferential sites’). Another possibility is that these stably bound complexes are a population of inactive Cy5-UvrA molecules that aggregated on the DNA after binding.

A small number of events were observed (ten in total), where DNA binding (and dissociation) was directly detected. Examples of UvrA directly binding to DNA are shown in Figures 8C and 8D. Remarkably, these complexes did not show any detectable diffusion along the DNA, but instead remained immobile after associating with DNA. An example of such a complex is shown in Figure 8C. In some events, the complex dissociated before the end of the imaging sequence, two examples of such complexes are shown in Figure 8D.

The immobility and stability of these complexes, directly upon binding DNA, suggest that these are also bound to a preferential site. However, it is very unlikely that UvrA can find these sites without probing the DNA for damage, even though it appears that the complexes have immediately bound a damaged site. Possibly, a searching UvrA complex is too fast to be detected with our TIRF microscopy setup. A transiently binding and dissociating protein would likely not stay bound for long enough to be properly imaged. For example, a fast sliding protein would appear as a faint blur on the images, if detected at all, because its fluorescent signal is spread out between the different positions the protein occupied during imaging. However, as most complexes observed with TIRF bound the DNA during the entire image sequence, we could not determine the lifetime of the UvrA complex on the preferential sites and calculate a possible lifetime of the UvrA-complex on a non-specific site.

Comparison of different surface modification techniques

One of the key issues in imaging protein-DNA interactions with TIRF-microscopy techniques is the flow cell surface (reviewed in [25]). The flow cell surface should be modified to allow DNA tethering, but also to prevent adsorption of fluorescent molecules and proteins. Many times, we observed the adsorption of either DNA or protein to the surface (examples are shown in Figure 9). Therefore, we tried different strategies for surface modification to overcome these limitations.

The results discussed above were obtained using a linear PEG coating, covalently attached to a poly-lysine amino-functionalized glass coverslide. Generally, this type of coating is optimal for DNA stretching and also has the lowest degree of surface adsorption of UvrA. Still, surface adsorption of UvrA did occur with this coating, exemplified in Figure 7, where UvrA molecules were visible at positions clearly not overlapping with DNA. Moreover, this type of coating appeared very difficult to reproduce, on many occasions DNA stretching could not be achieved because the DNA stuck to the glass slide. Likely, this problem with reproducibility is the result of variation in the density of the PEG-layer between different preparations.

Therefore, we also tried other coatings that have been used for similar purposes: Star-PEG-coating and BSA-coating. Although on these coatings DNA stretching was easier to reproduce, adsorption of UvrA was too high to validate binding to DNA (Figure 9). The introduction of an extra surface-blocking step (with 2 % acetylated BSA + 2 % casein) after the surface coating did reduce the non-specific adsorption of protein considerably, but not enough to verify DNA binding by UvrA.

Furthermore, the BSA-coating introduced relatively more fluorescent contaminants on the surface than the other coating methods, which makes it more difficult to discriminate YOYO-stained DNA and fluorescent protein from the background signal.

We also tried to form a PEG coating on a APTES (amino-silane) amino-functionalized glass coverslide (as used by Bonnet *et al.* [8]). DNA stretching was more reproducible on APTES-PEG coated glass slides than on PLL-PEG coating glass slides, but also on APTES-PEG surface adsorption of UvrA was an issue. Notably, all the methods we tried for surface coating have been successfully used for TIRF-microscopy based studies of other protein-DNA interactions. Likely, the unique nature and relatively large size (220 kDa) of the UvrA dimer makes this protein more susceptible to surface adsorption.

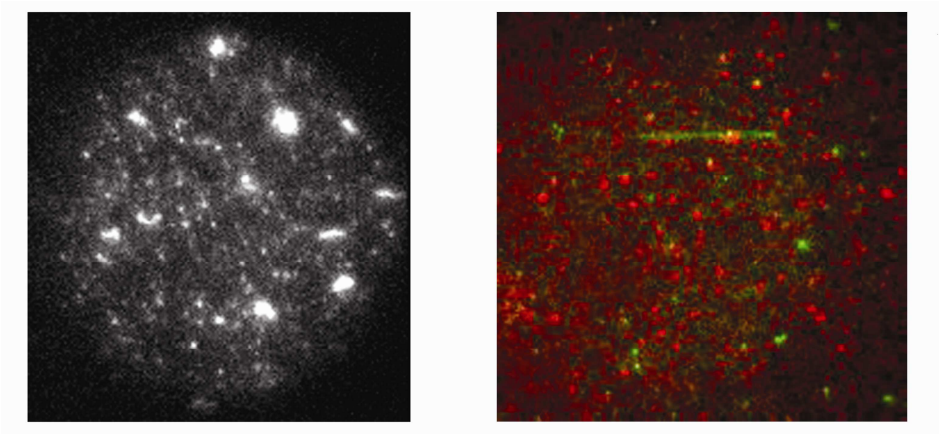

Figure 9: Examples of aggregated DNA and proteins on a glass surface
(**Left**): Formation of DNA aggregates on a coated glass surface. This particular image was recorded on poly-lysine + PEG coated glass. Image size: 50 × 50 μm. (**Right**): UvrA sticking to non-specific sites at the surface. In this case, the position of the majority of Cy5-UvrA does not overlap with the position of YOYO-stained DNA. This particular image was recorded in star-PEG coated glass. Image size: 30 × 30 μm.

Imaging of UvrA binding to DNA tethered between two optically trapped beads

To avoid undesirable surface interactions, we tried to observe the interaction of UvrA with DNA in a different experimental setup. Here, DNA is tethered between two optically trapped beads far from a flow-cell surface and imaged by farfield fluorescence microscopy. Before and during the incubation of DNA, the position of the two trapped beads was chosen such that the DNA was under a constant tension of approximately 20 pN. A stretching force of 20 pN indicates that the DNA substrate is stretched between the beads and has a length expected for B-DNA. Forces lower than 20 pN allow for longer thermal fluctuations of the DNA, which makes localization of the protein less accurate [26]. With this setup, we have succeeded to image UvrA-complexes binding DNA.

In the presence of ATP UvrA makes a stable interaction with preferential sites

To obtain the binding kinetics of UvrA, DNA was incubated for different times in buffer containing 2.5 nM Cy5-UvrA. After incubation, the DNA was transferred back to the buffer channel and imaged until most of the complexes had disappeared (this can be either due to fluorophore bleaching or dissociation of UvrA). The amount of UvrA-complexes visible on the first image was counted manually. When UvrA was incubated in the presence of ATP, there was no linear correlation between the incubation time and the amount of complexes (Table 3). An incubation time of 5 seconds resulted in (on average) six UvrA complexes per DNA molecule, but a 40 times longer (200 sec) incubation time did not result in 40 times more UvrA complexes on the DNA (Figure 10A).

Instead, the amount of UvrA complexes bound seemed to be limited to approximately 14 per DNA molecule, and this number is already reached after 20 seconds incubation. This non-linear relationship between the amount of complexes and the incubation time argues against the existence of an inactive population of UvrA complexes that would aggregate on the DNA. If such a population would exist, these aggregates would likely accumulate on the DNA over time and this is not observed.

This result suggests that we observed UvrA binding to specific preferential sites within the DNA, similar to what was observed with TIRF. These sites would then all be found within 20 seconds. Another possibility is that we observed UvrA binding to non-specific DNA sites, which then should reach a binding equilibrium within 20 sec.

To discriminate between these two possibilities, we determined the lifetime of the UvrA-DNA complexes. To determine the contribution of fluorophore bleaching to the observed lifetime of the protein complex, we imaged UvrA using two different illumination protocols: continuous illumination and stroboscopic illumination. In the continuous illumination protocol, the laser was continuously on and each 0.5 sec an image was recorded. In the stroboscopic illumination protocol, the laser gave a pulse (lasting 0.5 sec) every 5 sec, thus making one image per 5 sec. With continuous illumination, the amount of fluorophore bleaching is higher, but, due to the better time resolution, it allows a more accurate observation of changes in the position of the complex.

The average lifetime of the UvrA-DNA complex was obtained by manually counting the number of UvrA complexes present in each subsequent image. To calculate the lifetime, these results were initially fitted to a single exponential curve (Figure 11).

Table 3: Average number of Cy5-UvrA complexes on DNA, after different incubation times

Incubation time (sec)	UvrA + ATP	UvrA + ATPγS
1	N.D.	11 (3 DNA counted)
5	6 (4 DNA counted)	~ 50 (1 DNA)
20	14 (10 DNA)	> 200 (1 DNA)
80	13 (2 DNA)	N.D.
200	11 (1 DNA)	> 200 (fully occupied) (4 DNA)

DNA stretched between two optically trapped beads was incubated with 2.5 nM Cy5-UvrA in 1x endo buffer plus oxygen scavengers, ATP or ATPγS was present in a concentration of 1 mM. The number of Cy5-UvrA complexes visible on each DNA molecule, in the first frame of the recorded movie, was counted manually.
N.D.: Not Determined

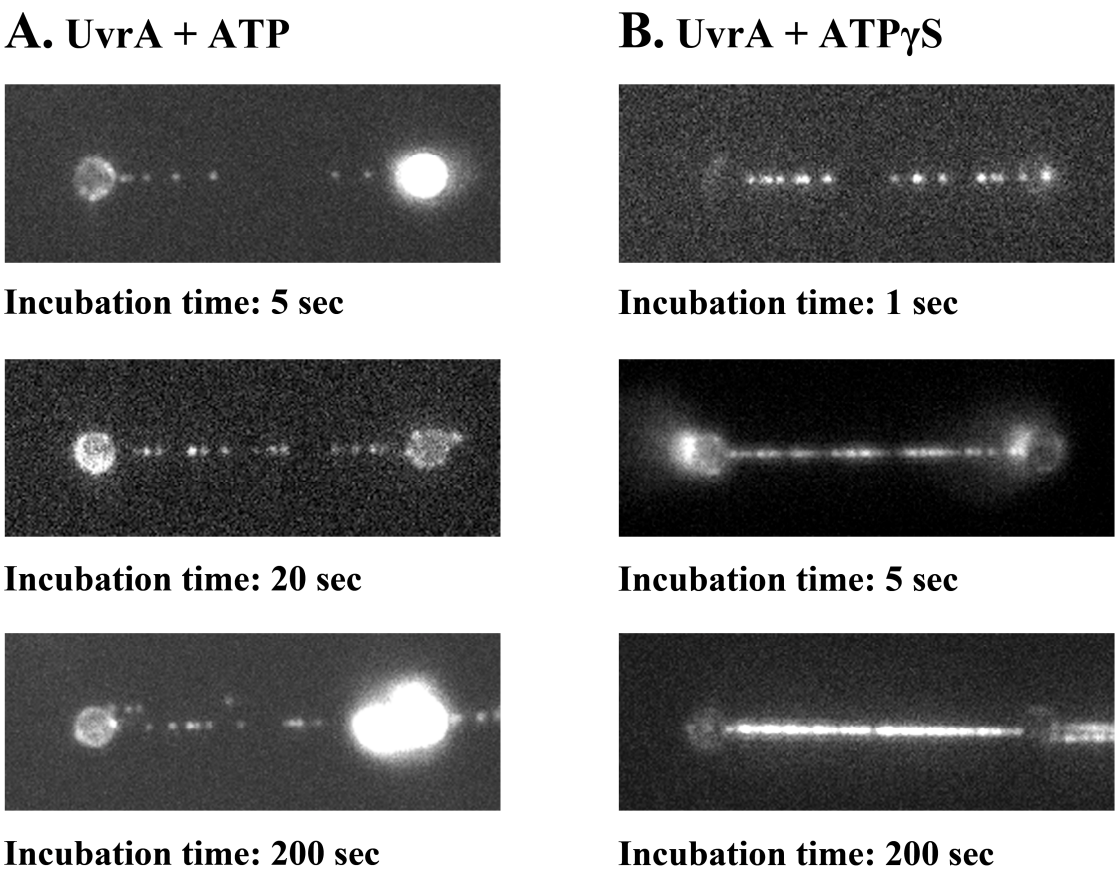

Figure 10: Screenshots of Cy5-UvrA bound to λ-phage DNA tethered between two optically trapped beads
The large circles on the edges of the screenshots are the trapped beads. The distance between the beads is approximately 16 μm, which is the length of stretched λ-phage DNA (48,000 bp). Because of the large size of the beads, fluorescent molecules will accumulate on the beads during the incubation. Each image was taken from the first image of the sequence. Sometimes (as shown in the screenshot from the 200 sec incubation in the presence of ATP) more than one DNA molecule was attached to the beads. All experiments were done at 20 °C, in the presence of a 0.2x concentrated oxygen scavenging system plus 2 mM Trolox.

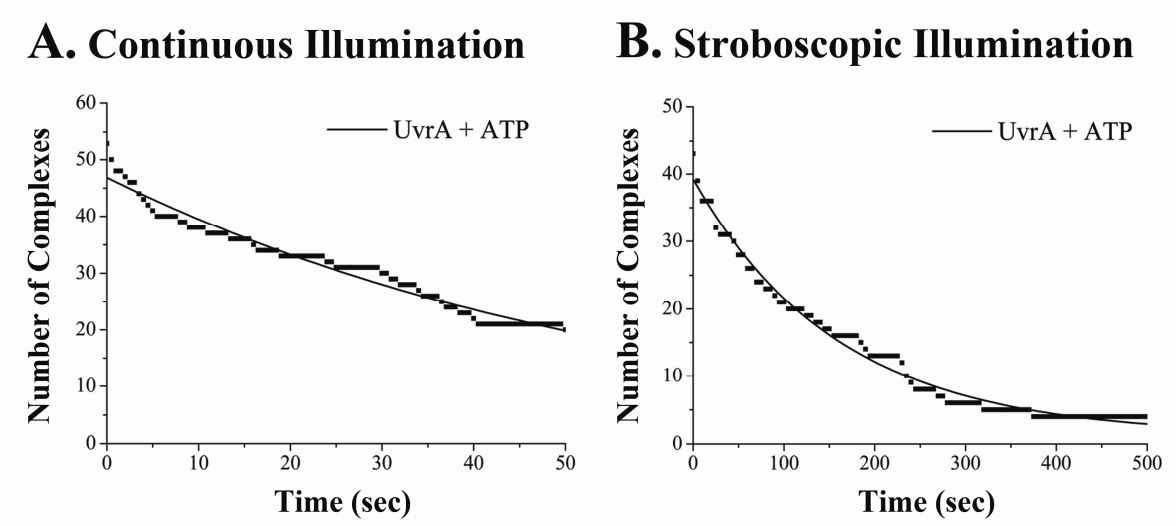

Figure 11: Amount of UvrA complexes bound to DNA during imaging

For at least four different incubations, the amount of complexes visible on each successive image was counted. With continuous one image was recorded every 500 msec; with stroboscopic illumination the DNA was imaged once every 5 seconds, with a 500 msec laser pulse. Second-order exponential fits were used to obtain the half-life of the UvrA-DNA complex. Curve fitting was done with OriginPro 8 software (OriginLab).

However, UvrA had a shorter half-life when imaged with continuous illumination (40 ± 10 sec) than when imaged with stroboscopic illumination (110 ± 20 sec) (Figure 11). This indicates that, with continuous illumination, the life-time of the Cy5-UvrA signal is determined by fluorophore bleaching rather than dissociation of UvrA. The half-life determined with stroboscopic illumination should however be dominated by dissociation of UvrA, as within 110 sec of stroboscopic illumination Cy5-UvrA has been exposed to the laser light for only 11 sec, which is significantly shorter than the half-life obtained with continuous illumination (40 sec). Adding the obtained bleach time (the half-life of Cy5-UvrA during continuous illumination, which would be 400 sec with stroboscopic illumination) as a second parameter to the exponential curve fit demonstrated that, during stroboscobic illumination, fluorophore bleaching accounted for less than 1 % of the signal decay. With a similar procedure, we determined that dissociation of UvrA accounted for about 2 % of the signal decay measured with continuous illumination. Moreover, these results suggest that in the presence of ATP the UvrA-DNA complex has a half-life of approximately 110 sec.

The obtained lifetimes suggest that UvrA makes a stable interaction with the DNA substrate and argue against DNA binding reaching equilibrium within an incubation time of 20 seconds. Therefore, both the non-linear relation between the number of complexes and incubation time with DNA and the long lifetime of the UvrA-DNA complexes indicate that we have observed UvrA bound to preferential sites (lesions) on the DNA substrate. On average, about 14 of such sites are present in each λ-phage DNA molecule.

To detect any changes in the position of the DNA-bound UvrA-complexes, kymographs were made from each image sequence (Figure 12A). Most of the UvrA complexes were immobile, similar to what was observed with TIRF-microscopy. Only one mobile UvrA complex was observed and this particular complex was observed with stroboscopic illumination (Figure 12A, bottom right panel). Between two consecutive images (here: 5 sec), this complex moved between two binding sites that were about 1.25 μm (3750 bp) apart. As this particular complex had a long residence time on both sites and the buffer did not contain UvrA, it has likely moved between two preferential sites.

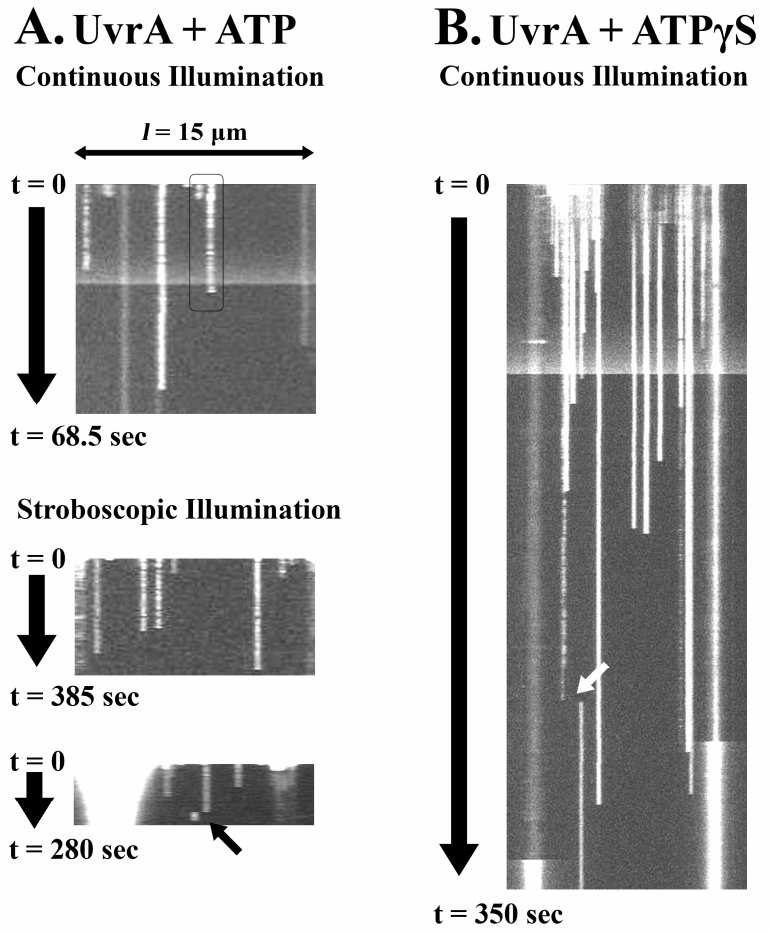

Figure 12: Examples of kymographs of UvrA position on stretched DNA

(**A**) Kymographs of UvrA incubated with ATP, imaged with continuous or stroboscopic illumination

(**B**) Kymograph of UvrA incubated with ATPγS

The small arrows indicate 'jumping' events in which, within the time to record one image, the UvrA complex moved between two different binding sites. The large spot visible in the bottom kymograph of panel A is the result of dust attaching to the tethered DNA during incubation. With continuous one image was recorded every 500 msec; with stroboscopic illumination the DNA was imaged once every 5 seconds, with a 500 msec laser pulse. The variations in signal intensity and sharpness are due to changes in the position of the laser focus. The highlighted complex is further analyzed in Figure 13. The kymographs were made using ImageJ software.

The changes in signal intensities seen on the kymographs are likely the result of fluorophore blinking. Analysis of the signal intensities of the complexes showed that a significant amount of the Cy5-UvrA complexes displayed stepwise bleaching of two (or more) fluorophores (Figure 13). This could indicate that, given the average labeling of 1.2 Cy5 per UvrA, these are dimer complexes bound to DNA. Previously, it was shown that only the UvrA dimer can make a stable contact with DNA [18].

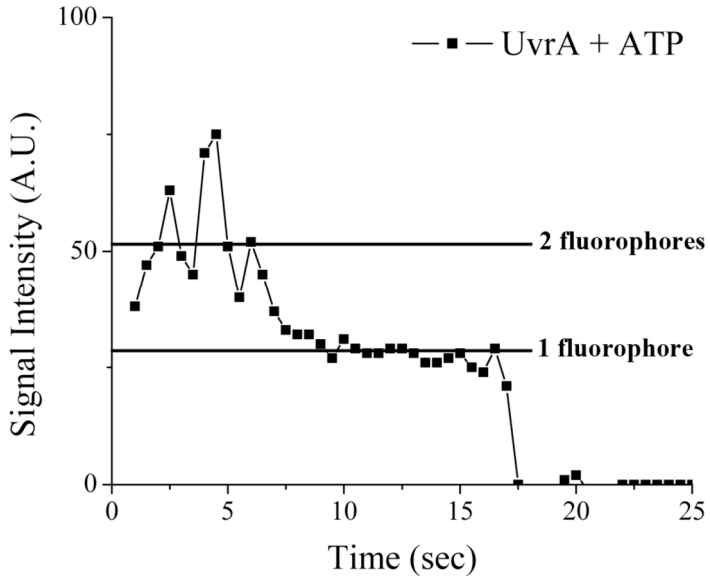

Figure 13: Step-wise bleaching of a Cy5-UvrA complex

The signal intensity of this Cy5-UvrA reveals a step-wise bleaching pattern, revealing the presence of two dyes in this particular complex. This particular complex is the second complex from the right in the top kymograph of Figure 12A (the complex is indicated with the gray rectangle). The two lines in this figure serve as a guide to the eye, to indicate the average signal intensity of one and two fluorophores.

In the presence of ATPγS UvrA binds stably to non-specific sites

We also imaged UvrA binding DNA in the presence of ATPγS (Figure 10B). In contrast to in the presence of ATP, in the presence of ATPγS UvrA-complexes accumulate on the DNA over time (Table 3). Moreover, already after 5 seconds many more complexes were observed on the DNA in the presence of ATPγS than in the presence of ATP. Notably, after 200 seconds, the DNA was fully occupied by UvrA (Figure 10B, bottom panel). The observed accumulation of UvrA in time strongly suggests that, with ATPγS, we are observing UvrA binding to non-specifically to DNA.

From earlier studies it is known that with ATPγS UvrA preferentially binds DNA ends and DNA damage, although recognition of internal DNA lesions is reduced compared to UvrA in the presence of ATP [18].

Therefore, in the presence of ATPγS, UvrA is still capable of site-specific binding and could be expected to slide towards a preferential site. However, the bulk of the observed complexes are not mobile on the DNA (Figure 12B) and bound very stably, having a half-life of 90 ± 45 sec. This suggests that, in this condition, UvrA does not find lesions or DNA ends by sliding along non-specific sites. Out of the approximately 500 observed complexes, two mobile complexes were detected. One example is shown in Figure 12B, on the left kymograph. On this kymograph, a UvrA complex moves between two binding sites, travelling approximately 1.75 μm (5000 bp) within in one frame (here: 0.5 sec). The most likely explanation for this motion is that, here, after dissociating from DNA UvrA has reached a new binding site by 3D-diffusion.

In the presence of ADP, UvrA does not make a stable interaction with DNA

We have also tried to observe the interaction of UvrA with DNA in the presence of ADP. However, in our initial trials no UvrA complexes were detected on the DNA. This is not unexpected as UvrA is known to have a greatly reduced affinity for DNA when bound to ADP; in the presence of ADP, UvrA has an approximately 100 times lower affinity for DNA than in the presence of ATP [27-29]. As we found a half-life of 110 seconds for the UvrA-DNA complex in the presence of ATP, it is very likely that in this condition all the complexes dissociated during the transport of DNA to the imaging buffer (this took about 5 seconds), before imaging could be started.

DISCUSSION

Using two single-molecule fluorescence imaging techniques, we have visualized UvrA binding to DNA. The imaging of UvrA-DNA complexes with farfield fluorescence was the most practical and reproducible technique. Although with TIRF-microscopy we could directly observe the formation of a UvrA-DNA complex and image Cy5-UvrA on a shorter timescale than farfield microscopy, problems with surface adsorption of either protein or DNA prevented us from generating more data. Furthermore, because in the farfield fluorescence microscopy setup the position of the DNA is more confined due to the optical trapping system, with this setup the position of UvrA on DNA can be more accurately determined than with the used TIRF-microscopy setup. Even though each technique has its specific imaging advantages and disadvantages, we found clear similarities between the results obtained with both techniques.

In both experiments, the large majority of UvrA molecules appeared to be immobile on the DNA. We have presented several lines of evidence that these immobile UvrA complexes do not represent an inactive population of fluorescent proteins that have aggregated on the DNA.

First, in the gel shift assays, the Cy5-labeled UvrA showed a similar DNA binding and UvrB loading activity as non-labeled UvrA and it also had a similar specificity for DNA damage and DNA ends. This argues against the existence of a large population within the Cy5-UvrA that would aggregate after binding DNA. Second, in our single-molecule experiments, the activity of Cy5-UvrA depended on the cofactor present, since there was clearly a difference in the activity of Cy5-UvrA in the presence of ATP and ATPγS. Inactive, aggregated, UvrA would likely not respond to changes in experimental conditions. Third, in the presence of ATP, a longer incubation time did not increase the amount of UvrA on the DNA. This also argues against aggregation of UvrA on DNA, as aggregates would likely accumulate on the DNA over time and we did not detect this.

Instead, we propose that the immobile UvrA complexes observed in the presence of ATP have bound to preferential sites within the substrate. These preferential binding sites are most likely DNA lesions resulting from the modification of the DNA substrate. These can be oxidative lesions, UV-induced damage, DNA nicks or lesions induced by physical stress on the DNA. Based on the half-life time of the UvrA complexes on specific sites (110 sec) and the assumption that these sites, although we do not know their exact nature, are more similar to CPD lesions than to ‘bulky’ synthetic lesions, the half-life time of UvrA on a non-specific site can be estimated as 100- to 1000 times lower than that of UvrA on a specific site, ranging between 0.1 and 1 second (UvrA binds a CPD damage about 1250 times more stably than a non-specific site [15]). This indicates that, after transport to the imaging channel, which takes about 5 seconds, all complexes on non-specific sites will have dissociated and will not be imaged.

With farfield fluorescent microscopy, non-specific binding might however be observed by imaging the DNA during the incubation with UvrA, although this would require the use of a lower concentration of fluorescent protein to reduce background fluorescence. But then also, a lifetime shorter than 1 second would mean that, in our farfield microscopy setup, the complex on a non-specific site would be only visible in 1 or 2 images of 500 msec continuous illumination.

With TIRF microscopy, DNA binding of UvrA could be imaged directly and on a faster timescale, but also with this technique, no complexes on non-specific sites were detected, either because the complex binds too brief to a non-specific site, or because it diffuses too fast on the DNA to be properly imaged.

In the presence of ATPγS, UvrA behaves different than in the presence of ATP. In the presence of ATPγS, UvrA accumulated non-specific sites and bound these much more stably than in the presence of ATP, suggesting that in this condition UvrA does not preferentially bind DNA lesions. However, with AFM we have shown that in this condition UvrA did not accumulate on DNA and was still able to find DNA ends with a similar efficiency as with ATP (Table 2 and [18]). However, we did find that in the presence of ATPγS Cy5-UvrA did have a lower specificity for DNA ends, with respect to non-labeled UvrA (Table 2). Although Cy5-UvrA is not completely incapable of recognizing ends in this condition (40 % of the complexes did bind to a DNA end), the presence of ATPγS may very well affect the function of Cy5-UvrA. However, more data are needed to understand the discrepancy between the AFM and fluorescence microscopy results.

Three events were observed in which a UvrA complex 'jumped' between two distant binding sites. Likely, in these events the UvrA-complex has performed 3D-diffusion. The Stokes-Einstein relationship for diffusion of spherical particles in normal liquids reads: $D = k_B T / 6\pi\eta R_H$ (in which η presents the viscosity of the buffer ($1 \cdot 10^{-3}$ Pa·s for aqueous buffers) and $k_B T$ represents the thermal energy in one molecular degree of freedom ($4 \cdot 10^{-21}$ J under conditions relevant for UvrA) [30]. According to this formula, the UvrA dimer, being a 200 kDa complex with a hydrodynamic radius (R_H) of 6 nm [31], would have a 3D-diffusion constant (D) of about 40 μm^2/sec. This value suggests that, within 100 msec, the mean square 3D-displacement ($\langle x \rangle$) of the UvrA dimer would be about 2 μm or 6000 bp (according to $\langle x \rangle^2 = 2Dt$). This number is in agreement with the distances that the jumping UvrA complexes have traveled along the DNA (1.25, 1.75 and 2.2 μm respectively). The low density of DNA in our setup likely explains why we have seen only a small number of these events, as the chance that a UvrA dimer rebinds to the stretched DNA after dissociation will be very small, as the DNA substrate only occupies a small part of the volume in which the UvrA dimer can diffuse [2]. In the living cell on the other hand, the concentration of DNA is likely much higher, which increases the chance of rebinding DNA after dissociation.

ACKNOWLEDGEMENTS

This work was supported by the Netherlands Organization for Scientific Research (NWO) [grant number 700.52.706]. The authors would like to thank Wiepke Koopmans for building the TIRF-microscopy setup and for his assistance with operating the TIRF-microscope. Remus Dame is kindly acknowledged for his assistance in setting up the collaboration between the workgroups at Leiden University and VU Amsterdam.

REFERENCES

1. Truglio, J.J., Croteau, D.L., Van Houten, B. and Kisker, C. (2006) Prokaryotic Nucleotide Excision Repair: The UvrABC system. *Chem. Rev.*, **106**, 233-252

2. Halford, S.E. and Marko, J.F. (2004) How do site-specific DNA-binding proteins find their targets? *Nucleic Acids Res.*, **32**, 3040-3052

3. Riggs, A.D., Bourgeois, S. and Cohn, M. (1970) The *lac* repressor-operator interaction. III. Kinetic studies. *J. Mol. Biol.*, **53**, 401-417

4. Winter, R.B. and von Hippel, P.H. (1981) Diffusion-driven mechanisms of protein translocation on nucleic acids. 2. The *Escherichia coli* repressor -- operation interaction: equilibrium measurements. *Biochemistry*, **20**, 6948-6960

5. Winter, R.B., Berg, O.G. and von Hippel, P.H. (1981) Diffusion-driven mechanisms of protein translocation on nucleic acids. 3. The *Escherichia coli* repressor -- operation interaction: kinetic measurements and conclusions. *Biochemistry*, **20**, 6961-6977

6. Berg, O.G., Winter, R.B. and von Hippel, P.H. (1981) Diffusion-driven mechanisms of protein translocation on nucleic acids. 1. Models and theory. *Biochemistry*, **20**, 6929-6948

7. Tafvizi, A., Huang, F., Leith, J.S., Fersht, A.R., Mirny, L.A. and van Oijen, A.M. (2008) Tumor suppressor p53 slides on DNA with low friction and high stability. *Biophys. J.*, **95**, L01-L03

8. Bonnet, I., Biebricher, A., Porte, P.L., Loverdo, C., Benichou, O., Voituriez, R., Escude, C., Wende, W., Pingoud, A. and Desbiolles, P. (2008) Sliding and jumping of single EcoRV restriction enzymes on non-cognate DNA. *Nucleic Acids Res.*, **36**, 4118-4127

9. Blainey, P.C., van Oijen, A.M., Banerjee, A., Verdine, G.L. and Xie, X.S. (2006) A base excision repair protein finds intrahelical lesion bases by fast sliding in contact with DNA. *Proc. Natl. Acad. Sci. U.S.A.*, **103**, 5752-5757

10. Gorman, J., Chowdhury, A., Surtees, J.A., Shimada, J., Reichman, D.R., Alani, E. and Greene, E.C. (2007) Dynamic basis for one-dimensional DNA scanning by the mismatch repair complex Msh2-Msh6. *Mol. Cell*, **28**, 359-370

11. Axelrod, D. (1981) Cell-substrate contacts illuminated by total internal reflection fluorescence. *J. Cell Biol.*, **89**, 141-145

12. van Mameren, J., Modesti, M., Kanaar, R., Wyman, C., Wuite, G.J.L. and Peterman, E.J.G. (2006) Dissecting elastic heterogeneity along DNA molecules coated partly with Rad51 using concurrent fluorescence microscopy and optical tweezers. *Biophys. J.*, **91**, L78-L80

13. van Mameren, J., Peterman, E.J.G. and Wuite, G.J.L. (2008) See me, feel me: methods to concurrently visualize and manipulate single DNA molecules and associated proteins. *Nucleic Acids Res.*, **36**, 4381-4389

14. Verhoeven, E.E.A., van Kesteren, M., Turner, J.J., van der Marel, G.A., van Boom, J.H., Moolenaar, G.F. and Goosen, N. (2002) The C-terminal region of *Escherichia coli* UvrC contributes to the flexibility of the UvrABC nucleotide excision repair system. *Nucleic Acids Res.*, **30**, 2492-2500

15. Wagner, K., Moolenaar, G.F. and Goosen, N. (2010) Role of the two ATPase domains of *Escherichia coli* UvrA in binding non-bulky DNA lesions and interaction with UvrB. *DNA Repair*, **9**, 1176-1186

16. Sanbrook, J. and Russell, D.W. (2001) Molecular Cloning, a laboratory manual, 3rd edition. *CSHL Press*

17. Visse, R., de Ruijter, M., Moolenaar, G.F. and van de Putte, P. (1992) Analysis of UvrABC endonuclease reaction intermediates on cisplatin-damaged DNA using mobility shift gel electrophoresis. *J. Biol. Chem.*, **267**, 6736-6742

18. Wagner, K., Moolenaar, G., van Noort, J. and Goosen, N. (2009) Single-molecule analysis reveals two separate DNA binding domains in the *Escherichia coli* UvrA dimer. *Nucleic Acids Res.*, **37**, 1962-1972

19. Koopmans, W.J.A., Brehm, A., Logie, C., Schmidt, T. and van Noort, J. (2007) Single-Pair FRET microscopy reveals mononucleosome dynamics. *J. Fluoresc.*, **17**, 785-795

20. Koopmans, W.J.A., Schmidt, T. and van Noort, J. (2008) Nucleosome immobilization strategies for Single-Pair FRET microscopy. *ChemPhysChem*, **9**, 2002-2008

21. Groll, J., Ademovic, Z., Ameringer, T., Klee, D. and Moeller, M. (2005) Comparison of coatings from reactive star shaped PEG-*stat*-PPG prepolymers and grafted linear PEG for biological and medical applications. *Biomacromolecules*, **6**, 956-962

22. Xu, C., Losytskyy, M.Y., Kovalska, V.B., Kryvorotenko, D.V., Yarmoluk, S.M., McClelland, S. and Bianco, P.R. (2007) Novel, monomeric cyanine dyes as reporters for DNA helicase activity. *J. Fluoresc.*, **17**, 671-685

23. Cognet, L., Harms, G.S., Blab, G.A., Lommerse, P.H.M. and Schmidt, T. (2000) Simultaneous dual-color and dual-polarization imaging of single molecules. *Appl. Phys. Lett.*, **77**, 4052-4054

24. Rasband, W.S. (1997-2009) ImageJ, version 1.39, *U. S. National Institutes of Health, Bethesda, Maryland, USA*, http://rsb.info.nih.gov/ij/

25. Visnapuu, M.L., Duzdevich, D. and Greene, E.C. (2008) The importance of surface in single-molecule bioscience. *Mol. Biosyst.*, **4**, 394-403

26. Candelli, A., Gross, P. Wuite, G.J.L. and Peterman, E.J.G. (2009) Visualizing single proteins on a single DNA molecule with super-resolution. *Presented at 53rd annual meeting of the Biophysical Society*

27. Seeberg, E. and Steinum, A. L. (1982) Purification and properties of the UvrA protein from *Escherichia coli*. *Proc. Natl. Acad. Sci. U.S.A.*, **79**, 988-992

28. Van Houten, B., Gamper, H., Sancar, A. and Hearst, J.E. (1987) DNaseI footprint of ABC excinuclease. *J. Biol. Chem.*, **262**, 13180-13187

29. Mazur, S. and Grossman, L. (1991) Dimerization of *Escherichia coli* UvrA and its binding to undamaged and ultraviolet damaged DNA. *Biochemistry*, **30**, 4432-4443

30. Einstein, A. (1906) Über die von der molekularkinetischen Theorie der Wärme geforderte Bewegung von in ruhenden Flüssigkeiten suspendierten Teilchen. *Annalen der Physik*, **322**, 549–560

31. Orren, D.K. and Sancar, A. (1989) The (A)BC excinuclease of *Escherichia coli* has only the UvrB and UvrC subunits in the incision complex. *Proc. Natl. Acad. Sci. U.S.A.*, **86**, 5237-5241